Investigation of Progress in Dynamic Recrystallization in Two Austenitic Stainless Steels Exhibiting Flow Softening

A. Sarkar, J. K. Chakravartty[*]

Mechanical Metallurgy Division, Bhabha Atomic Research Centre, Mumbai, 400085, India

Abstract   The hot working behaviour of two austenitic stainless steels: SS304 and Ti-modified 15Cr-15Ni-2Mo (Alloy D9) were studied by hot compression test at temperatures of 900–1200°C and at strain rates of 0.002–1 s^{-1}. The progress of dynamic recrystallization (DRX) was modelled by the Avarmi kinetics equation. The flow softening was directly related to the DRX volume fraction and the DRX time was determined by strain rate. For quantification of recrystallization rate, the time corresponding to the DRX fraction of 50% was used. Analysis of the sigmoid-shaped recrystallization curves revealed that the rate of DRX increases with increasing deformation temperature and strain rate. Avrami exponents obtained indicated heterogeneous grain or twin boundary nucleation during DRX of these steels. Results of the Avrami analysis were used to predict the DRX flow curves for different deformation conditions.

Keywords   Austenitic Stainless Steel, Hot Compression, Dynamic Recrystallization, Flow Curve, EBSD, Microstructure

1. Introduction

Hot working is one of the important steps in fabrication of structural components used in various engineering applications. Dynamic recovery (DRV) and dynamic recrystallization (DRX) are the primary restoration mechanism during high temperature deformation of metallic materials. Micro mechanism of hot deformation in fcc metals and alloys is in general governed by their stacking fault energy (SFE). In some materials with high SFE such as aluminium, DRV can balance work hardening, and a plateau is achieved in the stress strain curves. However, in materials with low SFE such as austenitic stainless steels, the kinetics of DRV is low, and DRX can be initiated at a critical condition of strain energy accumulation. DRX is associated with softening in the stress-strain curves. DRX plays an important role in controlling microstructure and mechanical properties in hot working of many metallic materials[1–3]. Due to the great impact of DRX on the high temperature flow stress and its effect on the microstructure and properties of the material after processing, the evaluation of the rate and progress of DRX in terms of deformation conditions is of

utmost importance. The rate of DRX depends on the chemical composition of the material, the mode of deformation, and the deformation conditions.

In the present work, the rate and the progress of DRX in two stainless steels namely SS304 and a Ti-modified 15Cr-15Ni-2Mo austenitic stainless steel (known as alloy D9) were studied during hot compression test.

2. Experimental Procedures

Hot compression tests were conducted on solution-annealed (SA) SS304 and alloy D9 and specimens of 10-mm height and 5-mm diameter in a deformation dilatometer. The specimen was heated to the deformation temperature at a heating rate of 5°C/s and held there for 10 min. Single-hit hot compression tests were carried out at temperatures of 900-1200 °C with strain rates of 0.002–1 s^{-1} up to true strain of about 0.6.

3. Results and Discussions

3.1. Stress-strain Behavior

Flow curves obtained at different temperatures and at a strain rate of 0.01 s^{-1} for SS304 and alloy D9 are shown in Figure 1 a and b respectively.

---

* Corresponding author:
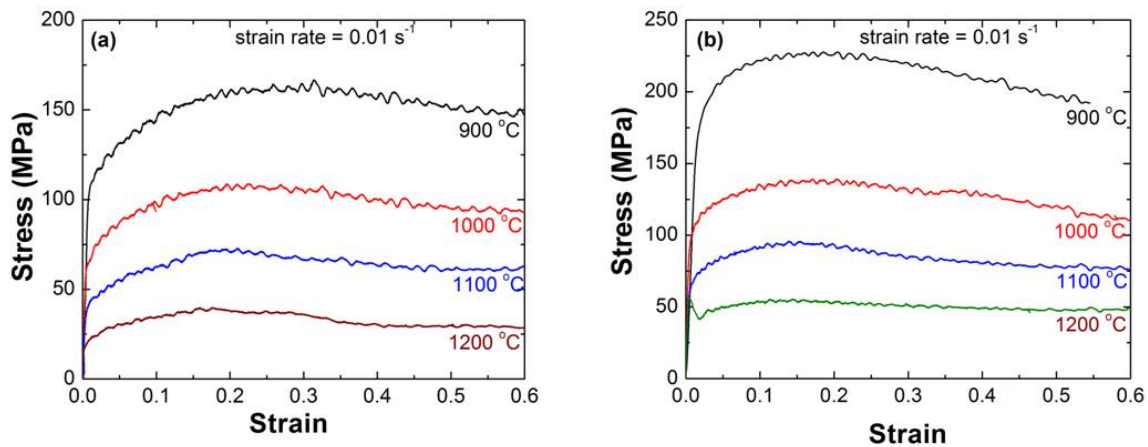jayanta@barc.gov.in (K. Chakravartty)

Figure 1. Stress-strain curves for (a) SS304 and (b) alloy D9 deformed at a strain rate of 0.01 s^{-1} at different temperatures

Most of the curves exhibit typical DRX behaviour with a single peak stress followed by a gradual fall towards a steady-state stress. However, the peak becomes less obvious when the strain rate increases or the deformation temperature decreases. The drop in flow stress with deformation temperature may be attributed to the enhancement in the rate of restoration processes and consequent decrease in the strain hardening rate. Since the formation of DRX nuclei becomes easier at higher deformation temperatures, the critical strain for initiation of DRX decreases. Moreover, the mobility of grain boundaries increases with increasing deformation temperature and hence the rate of DRX increases. Therefore, both the peak and steady state strains decrease with increasing the deformation temperature. The increase in the flow stress with strain rate can be ascribed to the decrease in the rate of restoration processes and increase in the strain hardening rate. The rate of DRV also decreases with increasing strain rates. Since the formation of DRX nuclei depends on the recovery substructures, the increase in the critical strain for initiation of DRX with increasing strain rate is expected. Moreover, the mobility of grain boundaries decreases with increasing strain rate, which in turn increases the peak and steady state strains. These observations are consistent with earlier observations on several alloy systems exhibiting flow softening during DRX[1-3].

3.2. Deformation Microstructure

The hot-deformed samples were cut along the longitudinal direction using a precision cut-off machine. One half of the sample was taken to prepare specimens for electron backscattered diffraction (EBSD) investigation. The microstructures were examined in the maximum deformation zone of the specimens. EBSD scans were performed on all processed samples using a TSL-Orientation Imaging Microscopy (OIM) system attached to an FEI Quanta 200 scanning electron microscope (FEI, Eindhoven, Netherlands) operating at 30 kV. Samples for EBSD were polished up to 0.25-lm grit diamond paste using the standard metallographic polishing procedure. Finally samples were

electro polished to ensure removal of any residual surface deformation. EBSD maps were collected from the processed samples using a step size of 0.5 µm using a hexagonal grid. Fig 2 shows the microstructure of the starting SS304 material.
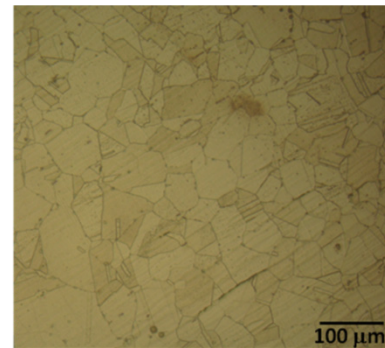

Figure 2. Optical microstructure of the starting annealed SS304 sample

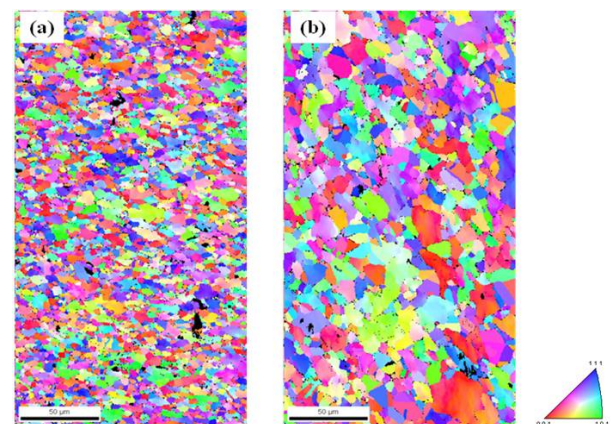Figure 3 a and b show the EBSD maps of the SS304 samples deformed at 900°C and 1000 °C

Figure 3. EBSD images of deformed SS304 samples at strain rate of 0.01 s^{-1} (a) 900°C (b) 1000 °C

Figure 4 shows the EBSD maps of the starting alloy D9 material and the samples deformed at 1000 and 1100°C at strain rate of 0.01 s^{-1}.
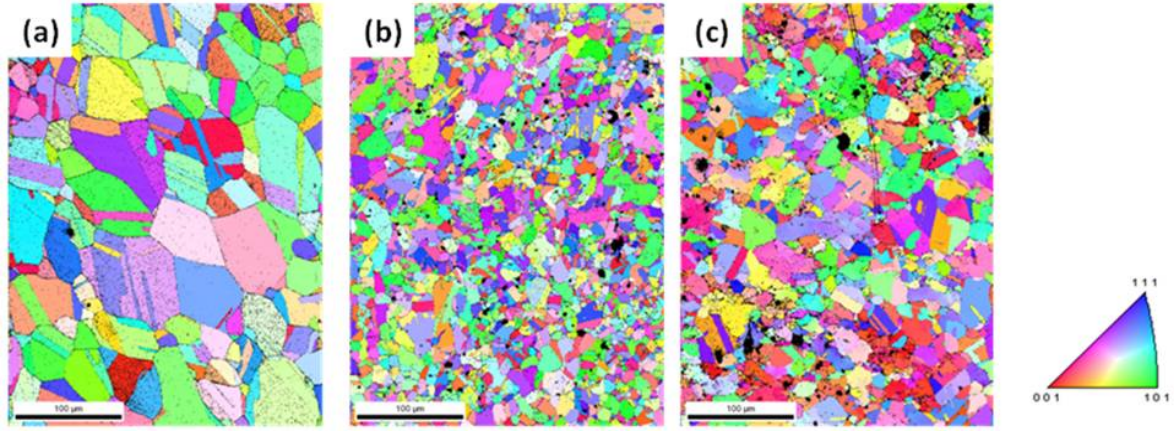
Figure 4.   EBSD images of (a) starting solution annealed alloy D9 and samples deformed at strain rate of 0.01 s^{-1} at (b) 1000°C (c) 1100°C

The starting solution annealed materials essentially comprised large grains (with an average diameter of about 35µm) along with large fraction of twin boundaries (Figure 2 and 4a). It is seen from the Figure 3a and 3b and 4 b and 4c that the initial structure is completely modified and the deformed microstructures consist of fine uniform grains. This is the typical characteristics of DRX. This type of microstructure modification and occurrence DRX during hot compression of steels has also been reported by Mandal et al.[4-7].

3.3. Avrami Analysis of Flow Curves

Avrami relation[8-10] is a popular approach to study how solids transform from one phase (state of matter) to another at a constant temperature. It can specifically describe the kinetics of a phenomena which is governed by nucleation and growth processes. It is generally accepted that the progress in DRX also follows Avrami equation. However, the study of DRX in terms of Avrami equation is not straight forward. Various computational methodologies have been proposed to predict DRX and microstructure evolution such as Vertex models[11], Potts-type Monte Carlo[12], phase field models[13] and cellular automata[14]. Results obtained from these simulation studies provided a reasonable understanding of the DRX kinetics. However, it is always advantageous to investigate the evolution of DRX from experimental flow behaviour. Recently Jonas et al.[15] has developed a novel formalism to investigate the Avrami kinetics of DRX. They analyzed various flow curves of different steels using their method. Here in this study we apply the formalism of Jonas et al. to investigate the DRX kinetics of alloy D9.

In this approach, an experimental flow curve is considered to be the net result of the simultaneous operation of dynamic recovery and DRX. This has been illustrated by schematic curves in Fig 5.

It explains the difference between the features of flow curves obtained during operation of dynamic recovery and DRX. DRX curve is obtained experimentally by carrying out compression tests at different strain rates and temperatures. However, the recovery curve (σ_{DRV}) which is regarded as

resulting from dynamic recovery alone is not available directly from the experiment. The recovery curve is assumed to represent the work hardening behavior of the unrecrystallized region. Now it is well known that during the deformation, DRX initiates after a certain critical stress (σ_c). The work hardening behavior of the recovery curve is same as that of the experimental curve prior to the critical strain (ε_c), where ε_c is strain corresponding to σ_c. The recovery curve finally reaches saturation (σ_{sat}) when there is a balance between the generation and annihilation rate of dislocation.
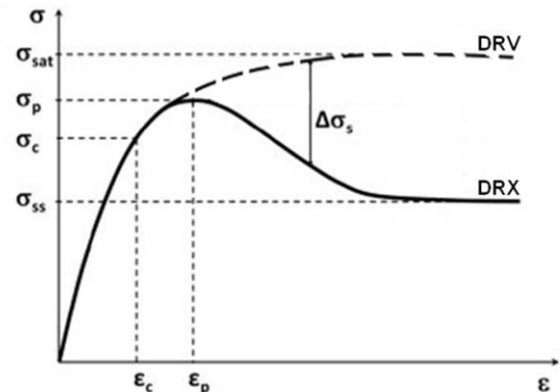

Figure 5.   Schematic representation of flow curves during dynamic recovery and dynamic recrystallization defining various stress and strain parameters involved in Avrami analysis

Identifying the ε_c and the corresponding σ_c is the first step toward DRX analysis. Flow curve analysis is now a well established technique for DRX analysis. The basis of the flow curve analysis method is that the DRX (as a restoration process) affects the flow curve shape by changing the rate of work hardening through the introduction of new strain free grains. To determine ε_c, we calculate the work hardening rate i.e. $\theta = d\sigma/d\varepsilon$ from the experimental data and plot against σ. The onset of DRX corresponds to a deviation in this work hardening curve. Fig 6a shows the typical plot of work hardening rate $\theta = d\sigma/d\varepsilon$ vs the flow stress σ for the D9 samples deformed at 1100°C at a strain rate of 0.002s^{-1}. These work hardening rate curves consist of two parts. The initial rapid decrease of θ with σ corresponds to dynamic recovery. The change of slope of this curve at a certain σ is

attributed to the initiation of dynamic recrystallization. Thus the change of slope in the work hardening curves is used to identify the critical stress σ_c and the corresponding critical strain ε_c. Poliak and Jonas[16] showed that the derivative of the work hardening rate ($-d\theta/d\sigma$) vs σ curve has a minimum at the inflection point of the work hardening curve. This is a better way to identify the σ_c. Inset in the Fig 6a show the plot of $-d\theta/d\sigma$ vs σ obtained from the experimental data.

In the approach of Jonas et al., the description of work hardening is based on the Estrin-Mecking[17] equation for evolution of dislocation density with strain:

$$\frac{d\rho}{d\varepsilon} = h - r\rho \qquad (1)$$

Where, h is the athermal work hardening rate and r is the rate of dynamic recovery. Based on this equation Jonas et al.[15] derived the equation for flow stress for dynamic recovery as:

$$\sigma = (\sigma_{sat}^2 - (\sigma_{sat}^2 - \sigma_0^2)\exp(-r\varepsilon))^{1/2} \qquad (2)$$

where σ_0 is the yield stress and can be determined from the experimental flow curve in terms of a 2% offset in the total strain.

Using some simple algebraic substitution they also obtained a useful relation:

$$\sigma\frac{d\sigma}{d\varepsilon} = \sigma.\theta = 0.5r\sigma_{sat}^2 - 0.5r\sigma^2 \qquad (3)$$

It can be seen from eqn (3) that r and σ_{sat} can be obtained respectively from the slope and intercept of $\sigma.\theta$ vs σ^2 curve.

Fig 6b shows a typical plot $\sigma.\theta$ vs σ^2 for alloy D9 deformed at 1100°C at a strain rate 0.002 s^{-1}. Fig 6c shows the corresponding work hardening or recovery curve obtained using the r and σ_{sat} values along with the experimental DRX curve.

The recrystallized volume fraction is considered to be responsible for the difference between the σ_{DRV} and σ_{DRX} curves. The difference between these two curves ($\Delta\sigma_s$) is the net softening and is directly attributed to DRX. The maximum value of $\Delta\sigma_s$ is ($\sigma_{sat} - \sigma_{ss}$), where σ_{ss} is the steady state stress under DRX conditions.. The evolution fractional softening with strain is expressed as $X = \Delta\sigma_s/(\sigma_{sat} - \sigma_{ss})$. Once

the recovery curve is derived for a particular deformation condition the evolution $\Delta\sigma_s$ with ($\varepsilon-\varepsilon_c$) can be obtained in a straightforward way.

The Avrami equation describing the SRX is expressed as:

$$X = 1 - \exp(-kt^n) = 1 - \exp\left(-0.693\left(\frac{t}{t_{50}}\right)^n\right) \qquad (4)$$

Here X represents the recrystallized volume fraction, k is the Avrami constant and n is termed as the Avrami time exponent. t_{50} is the characteristic time corresponding to 50% recrystallized volume fraction and is specified as[15]:

$$t_{50} = A\varepsilon^{-p}\dot{\varepsilon}^q d_o^v \exp\left(\frac{Q_{SRX}}{RT}\right) \qquad (5)$$

Here A is a constant, d_0 is the grain size, p, q and v are the strain, strain rate and grain size exponents respectively and Q_{SRX} is the activation energy for SRX.

We apply the same formalism to investigate the evolution of DRX in SS304 and alloy D9. Avrami plots of X vs ($\varepsilon-\varepsilon_c$) are derived for different deformation conditions. Figure 7 shows typical Avrami plots for SS304 deformed at 1200°C at a strain rate of 0.1 s^{-1}. Figure 8 shows the Avrami plots for alloy D9 samples deformed at strain rate of 0.002 s^{-1} at temperatures 900°C, 1000°C and 1100°C.

The Avarmi time exponents (n) obtained from the slope of the curves are shown in the figures. It can be seen that the values of n lie between 1.35-2.12 and increases with decreasing temperature. The low value ($\sim$1) of n indicates heterogeneous site saturated nucleation of recrystallized grains. On the contrary $n \sim$3, correlates with ideal Avrami recrystallization for homogeneous, constant rate nucleation[18]. The n values obtained in this study ($1<n<3$) signify that prior grain boundaries or twin edges are the nucleation cites for DRX in alloy D9. It is worth mentioning here that the detailed EBSD studies on the DRX behaviour of this steel by Mandal et al.[4-7] indicated heterogeneous nucleation at grain boundaries and formation of necklace structure. EBSD investigation also confirmed that twins play an important role during nucleation and subsequent expansion of the DRX process in alloy D9[5].
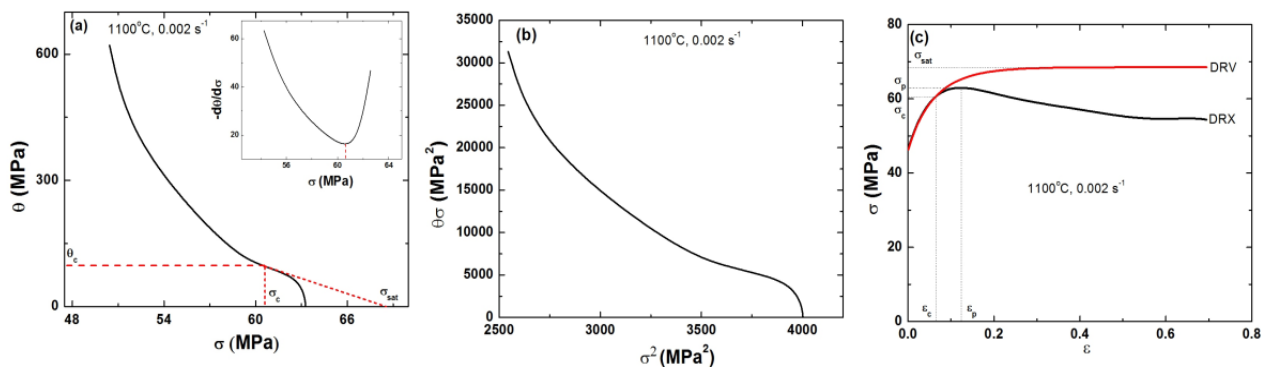

Figure 6. (a) θ vs. σ plot, (b) $\theta.\sigma$ vs. σ^2 plot and (c) reconstructed dynamic recovery (DRV) curve plotted along with the experimental dynamic recrystallization (DRX) curve for alloy D9 deformed at 1100°C, 0.002 s^{-1}
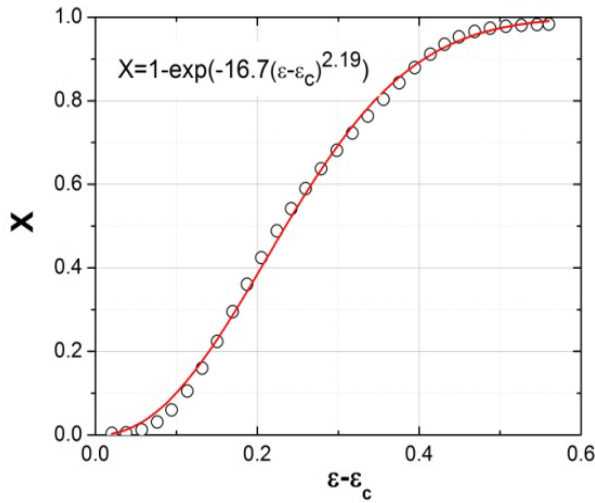
Figure 7. Variation of fraction recrystallization w.r.t. (ε-ε_c) for SS304 deformed at 1200°C at a strain rate of 0.1 s^{-1}
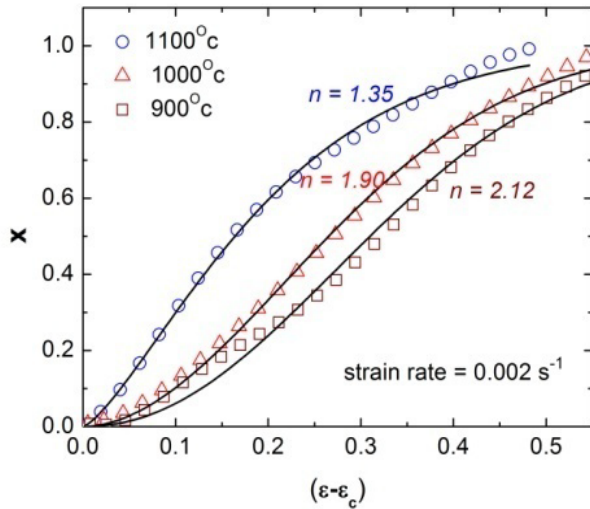

Figure 8. Variation of fraction recrystallization (X) w.r.t. (ε-ε_c) for alloy D9 at different deformation conditions

In Figure 9, the strain rate dependence of the characteristic time t_{50} for the flow curves determined at different temperatures is displayed for alloy D9. The value of the strain rate exponent q is ~ 1 and decreases with increasing temperature. The values of q are of the same order for that has been reported during the DRX of other fcc materials[15, 19] and are high compared to values reported in case of SRX[20].

The results of this analysis are also important as this will permit prediction of the DRX flow behavior at rates beyond that is achievable in laboratory test machines. This is significant from the industrial point of view for example to design the hot-forming process, predicting forming loads and power requirements at the relevant rates of deformation for alloy D9.
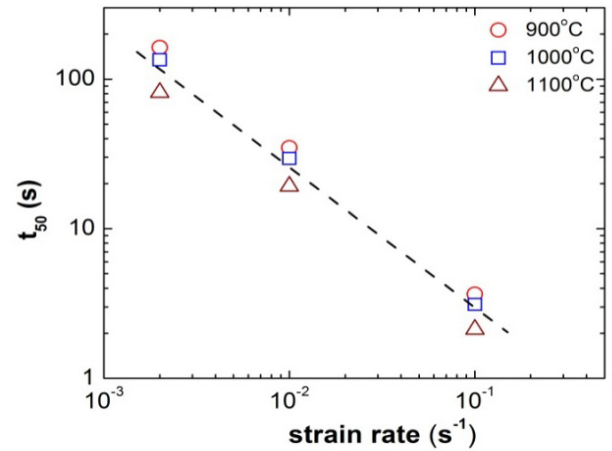

Figure 9. Dependence of the characteristic time (t$_{50}$) on strain rate (ε) for alloy D9

In order to generate the DRX flow curve at any desired rate of deformation it is required to establish the dependence of the parameters h and r on σ_p as has been suggested by Jonas et al.[15]. The various stress parameters associated with the DRX curve can be expressed in terms of σ_p using the experimental data. Figure 10 shows the variation of σ_{ss}, σ_{sat} and σ_c with σ_p for alloy D9.
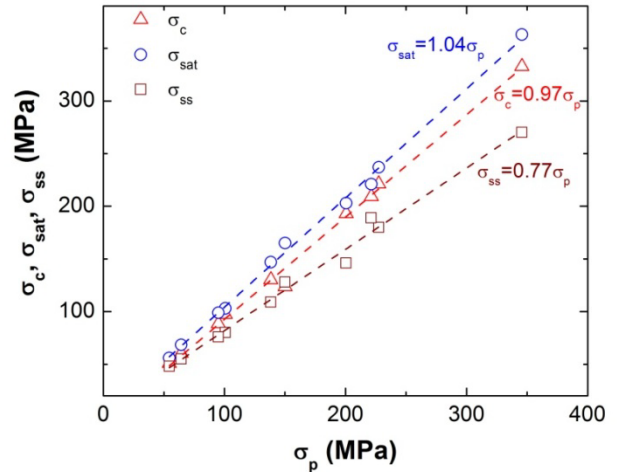

Figure 10. Plots showing the variation of critical stress (σ_c) and steady state stress for dynamic recovery (σ_{sat}) and steady state stress for dynamic recrystallization (σ_{ss}) with peak stress (σ_p) for alloy D9

A least square fit of the data gives the following relation between the stress parameters $\sigma_{ss} = 0.77\sigma_p$, $\sigma_{sat} = 1.04\ \sigma_p$, $\sigma_c = 0.97\ \sigma_p$. Similar relations have also been reported in other materials[15,21-24]. These relations will be useful for modeling purposes. Following Jonas et al.[15], the athermal work hardening parameter h can be determined using the relation:

$$h = r\frac{\sigma^2_{sat}}{(\alpha\mu b)^2} \qquad (6)$$

where α is a constant (taken as equal to 1)[15,25] and μ the shear modulus (81 GPa)[26] and b is the magnitude of Burgers vector (0.258 nm for alloy D9). Figure 11 shows the dependence of r and h on σ_p for alloy D9.
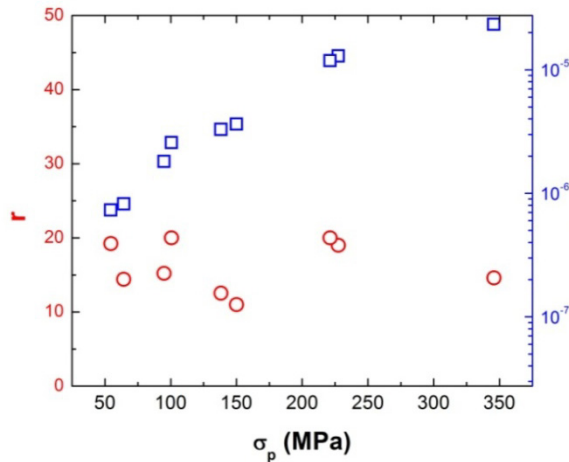

Figure 11. Dependence of the dynamic recovery coefficient r and the athermal work-hardening parameter h on σ_p for alloy D9

Now, σ_p can be related to T and by the well known relation:

$$Z = \dot{\varepsilon}\exp(Q/RT) = A'\left(\sinh(\alpha'\sigma_p)\right)^{n'} \qquad (7)$$

where is the Zener-Holomon parameter and Q is an activation energy. , and n' are constants derived from the nonlinear fit of the experimental data. Figure 12 shows the fit of Eqn. (7) to the experimental data. The best fit gives the values: $A' = 4.0^{10}$, $\alpha' = 0.0078$, Q = 284 kJ/mol and $n' = 5.43$.

The constants thus evaluated can be utilized to determine σ_p for alloy D9 at desired T and using Eqn. (7). Once the dependences of r, h and the other parameters on σ_p is established and the constants in Eqn. (7) are determined, it is possible to construct the DRV curve and subsequently the DRX curve for the desired deformation conditions of industrial processing. The predicted and the experimental DRX curve for different deformation conditions are shown in Figure 13.
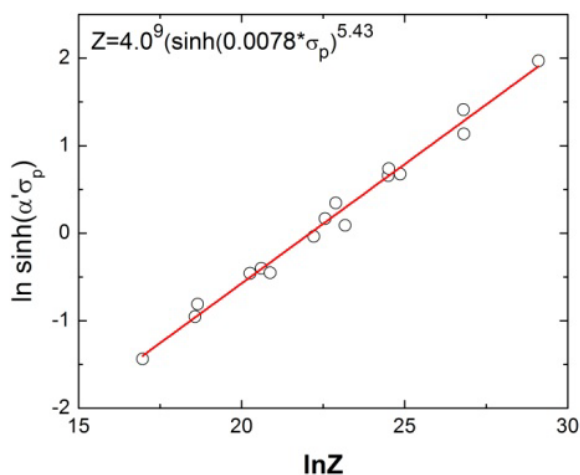

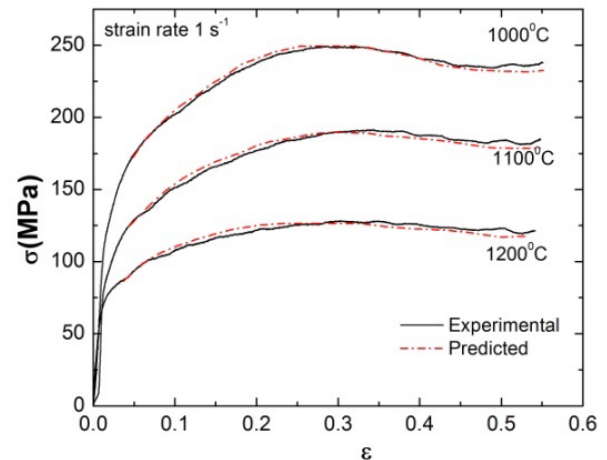
Figure 12. Plot of vs. lnZ

Figure 13. Predicted and experimental stress-strain curves for strain rate 1 s^{-1} at different temperatures for alloy D9

4. Conclusions

The DRX behavior of SS304 and Ti-modified austenitic stainless steel (alloy D9) are investigated under different deformation conditions through hot compression tests. The results of these tests are summarized as follows:

1. The stress–strain curves of SS304 and alloy D9 exhibited typical DRX behaviour with a single peak stress followed by a gradual fall towards a steady-state stress. At high temperature and low strain rate multiple oscillations were observed in the stress-strain curve.

2. The progress of DRX in the steels during hot deformation can be well predicted on the basis of the Avrami relation in conjunction with features of the flow curve and work hardening data.

3. The rate of DRX increases with deformation temperature. By increasing the deformation temperature, the recrystallization curve shifts to lower strains and recrystallization times.

4. The values of the Avrami exponent for different conditions ($1<n<3$) signify that prior grain boundaries or twin edges are the nucleation cites for DRX in these steels.

5. Flow curves for alloy D9 during hot working can be predicted well based on the analysis. These results will be useful to design the hot-forging/extrusion/rolling processes for alloy D9.

REFERENCES

[1]   T. Sakai, J. J. Jonas, Acta Metall., Vol. 32, 1984, p. 189.

[2]   A.Sarkar, R. Kapoor, A. Verma, J.K. Chakravartty, A.K. Suri, J. of Nuclear Mater., Vol. 422, 2012, p. 1.

[3]   J.K. Chakravartty, S. Banerjee, Y.V.R.K. Prasad, M.K. Asundi, J. of Nuclear Mater., Vol. 187, 1992, p. 260.

[4]   S. Mandal, A.K. Bhaduri, V. S. Sarma, Metal. Trans. A, Vol.

43, 2012, p. 2056.

[5]　S. Mandal, A.K. Bhaduri, V. S. Sarma, Metal. Trans. A, Vol. 43, 2012, p. 410.

[6]　S. Mandal, A.K. Bhaduri, V. S. Sarma, Metal. Trans. A, Vol. 42, 2011, p. 1062.

[7]　S. Mandal, P. V. Sivaprasad, V. S. Sarma, Mater. Manuf.Proc., Vol. 25, 2010, p. 54.

[8]　M. Avrami, J Chem. Phys. Vol. 7, 1939, p. 1103.

[9]　M. Avrami, J Chem. Phys., Vol. 8, 1940, p. 212.

[10]　W. A. Johnson, R. F. Mehl, Trans. AIME, Vol. 135, 1939, p. 416.

[11]　F.J. Humphreys, Scripta Metall. Mater., Vol.27, 1992, p. 1557.

[12]　D. Raabe, Computational Materials Science: The Simulation of Materials Microstructures and Properties, Wiley-VCH Verlag GmbH, D-69469 Weinheim, 1998.

[13]　L.Q. Chen, Y.Z. Wang, J. Miner., Met. Mater. Soc., Vol. 48, 1996, p. 13.

[14]　N. Yazdipour, C.H.J. Davies, P.D. Hodgson, Compt. Mater. Sci., Vol. 44, 2008, p. 566.

[15]　J. J. Jonas, X. Quelennec, L. Jiang, E. Martin, Acta Mater., Vol. 57, 2009, p. 2748.

[16]　E. I. Poliak, J. J. Jonas, Acta Mater., Vol. 44, 1996, p. 127.

[17]　Y. Estrin, H. Mecking, Acta Metall., Vol. 32, 1984, p. 57.

[18]　J. W. Cahn, Acta Metall., Vol. 4, 1956, p. 449.

[19]　C. Yue, L. Zhang, S. Liao, J. Pei, H. Gao, Y. Jia, X. Lian, Mater. Sci. Eng. A, Vol. 499, 2008, p. 177.

[20]　M.R. Barnet, G. L. Kelly, P. D. Hodgson, Metal. Mater. Trans. A, Vol. 33, 2002, p. 1893.

[21]　A. Dehghan-Manshadi and P. D. Hodgson, ISIJ International, Vol. 47, 2007, p. 1799.

[22]　C. M. Sellars, Czech. J. Phys. B, Vol. 35, 1985, p. 239.

[23]　N. D. Ryan, H. J. McQueen, Can. Metall. Q, Vol. 29, 1990, p. 147.

[24]　A. Sarkar, J. K. Chakravartty, B. Paul, A. K. Suri, Phys. Status Solidi (a), Vol. 208, 2011, p. 814.

[25]　X. Quelennec, N. Bozzolo, J. J. Jonas, R. Loge, ISIJ International, Vol. 51, 2011, p. 945.

[26]　H.J. Frost, M.F. Ashby, Deformation-mechanism maps: The plasticity and creep of metals and ceramics, Pergamon Press, Oxford, 1982.